Acta Mech Sin (2007) 23:689–698
DOI 10.1007/s10409-007-0100-7

RESEARCH PAPER

Centrifugal experimental study of suction bucket foundations under dynamic loading

Xiaobing Lu · Yongren Wu · Bintian Jiao · Shuyun Wang

Received: 13 November 2006 / Revised: 9 May 2007 / Accepted: 9 May 2007 / Published online: 4 September 2007

Abstract Centrifugal experiments were carried out to investigate the responses of suction bucket foundations under horizontal and vertical dynamic loading. It is shown that when the loading amplitude is over a critical value, the sand at the upper part around the bucket is softened or even liquefied. The excess pore pressure decreases from the upper part to the lower part of the sand layer in the vertical direction and decreases radially from the bucket's side wall in the horizontal direction. Large settlements of the bucket and the sand layer around the bucket are induced by dynamic loading. The dynamic responses of the bucket with smaller height (the same diameter) are heavier.

Keywords Centrifugal experiments · Suction bucket · Dynamic loading · Saturated sand

1 Introduction

A suction bucket foundation is a closed-top steel tube that is lowered to the seafloor, allowed to penetrate the bottom sediments under its own weight first, and then pushed to full depth with suction force produced by pumping water out of the interior. In recent years, suction bucket foundations have been used increasingly for gravity platform jackets, jack-ups [1–3]. They also have the potential of being used for several other purposes, such as offshore wind turbines, subsea systems and seabed protection structures [4–7]. The first advantage of suction bucket foundations are attractive because of the convenient method of installation and repeated use. For an example, a suction bucket foundation with a diameter of 9m and a height of 10m can be installed in 1–3 h, by using only a pump. The second advantage is that it may mobilize a significant amount of passive suction during uplift under some conditions, although the mobilisation of suction depends mainly on the loading rate and recommendations actually do not rely on the suction for design [8]. Although some studies about the installation and bearing capacity have been studied, the detail responses of the suction bucket foundations under dynamic loadings have remained unknown [9–11]. The dynamic loading condition is significant when suction buckets are used as the foundation of an offshore structure. Wave, ice or wind often exert cycle loading on the foundation [12,13]. The lack of experience with these loading conditions leads to a proposal for a test program to gain a deeper understanding. The considerable expense and time-consuming nature of prototype tests mean that the investigation of the bearing capacity of real scale devices is of limited practicality. However it is much easier to change parameters in small scale tests. The soil type may be varied in these cases. The dimensions of the suction bucket and other process parameters may be varied conveniently also. Nevertheless, in a small scale test, the problems arise concerning the stress-dependent behavior of soil that the measured loadings are so low that measurements are not sufficiently accurate to visualize differences in design. Because the behavior of soil is stress dependent and therefore the model in the small scale test and the prototype can not be subjected to the same stress level to exhibit the same responses. These restrictions can be overcome if performing the tests in a geotechnical centrifuge. In a centrifuge the soil stresses over a similar depth are the same as in the prototype situation. Centrifugal tests are "model" tests in that the results

The project supported by the fund of Chinese Ocean Oil Co. and Chinese Academy of Sciences(KZCX2-YW-302-02).

X. Lu (✉) · Y. Wu · B. Jiao · S. Wang
Institute of Mechanics, Chinese Academy of Sciences,
Beijing 100080, China
e-mail: xblu@imech.ac.cn

can be scaled up to the size of full-scale buckets. The main reason to select centrifugal test is the proper modeling of body forces, which are critically important for the full-scale prototype geotechnical problem, and for the capability of investigating both undrained and partially drained conditions.

Only a few field tests of suction bucket foundations have been reported in the open literature [14]. A number of investigators have tested scale models of suction buckets in geotechnical centrifuges [15,16].

Early experience with this technology often involved relatively stiff soils and axial compressive loads applied at the top center of the bucket. Centrifugal tests on suction piles were reported in Ref. [17]. Rate dependent loading tests on clay at 1g were performed by Jones et al. [18], Steensen-Bach [19].

Later designs for floating structures in the deeper water, where horizontal or inclined mooring lines are attached to a bucket, lead to the need for the increased lateral capacity. Although the offshore industry is deploying suction buckets in this configuration, a number of design issues remain unresolved [15,20].

The dynamic loading is transmitted to the soils by platform and causes the degradation of strength and modulus of the soil layers. As a result, the bearing capacity of bucket foundations decreases. Therefore, it is important to clarify the dynamic behavior of bucket foundations under dynamic loadings in order to provide practical design methods and parameters [21,22].

Although suction installation of bucket foundations is not clarified and is under investigation [23,24], the attention is concentrated on the responses.

2 Scaling law

In centrifugal experiments, the scaling law is important. Especially the conflict time scaling factors should be considered if the problem is related to the consolidation and dynamic loading.

Consolidation relates to the dissipation of excess pore pressure is a diffusion event. The degree of consolidation is described by the dimensionless time factor T_v defined as: $T_v = \frac{c_v t}{H^2}$, where c_v is the coefficient of consolidation, t the time and H a length related to a drainage path. It is easy to obtain the scaling factor of consolidation as $t_m = \frac{1}{N^2}\frac{c_{vp}}{c_{vm}} t_p$. Hence, if the same material is used in both model and prototype, the time scaling factor is $1 : N^2$. If for some reason the permeability in model and prototype is different, the time scaling relation becomes: $t_m = \frac{1}{N^2}\frac{k_p}{k_m} t_p$, where k_p, k_m are the coefficients of permeability in model and prototype, respectively [25].

Table 1 The main scaling factors

Parameters	Ratio of model to prototype
Length	$1/N$
Stress	1
Strain	1
Force	$1/N^2$
Acceleration	N
Frequency	N
Time (dynamic)	$1/N$
Time (seepage)	$1/N^2$

For the problems that the dynamic loading need considered, it is also easy to obtain the scaling factors of linear dimension, acceleration and frequency as: $1 : N$, $1 : N^{-1}$ and $f_m = N f_p$. An important consequence of this is that the time scaling factor for dynamic events is $1 : N$ in contrast to $1 : N^2$ time scaling factor for diffusion or seepage events.

The conflict time scaling factors require special consideration in the condition that both the dynamic effect and the seepage need considered. The method to ensure the same time scaling factor for motion and seepage usually decreases the effective permeability of solid material by increasing the viscosity of the pore fluid or by changing the grain series of solid material. The main scaling factors considered in the experiments are shown in Table 1.

In the present experiments, a new method is adopted. It does not change the materials according to the dimensionless analysis. We first discuss three dimensionless factors: the ratio of the cycle of the loading (period $\frac{1}{f}$) to the characteristic time of percolation $\left(\frac{H^2}{C_v} = \frac{\mu H^2}{KE(1+e)}\right)$, $\frac{KE(1+e)}{\mu H^2 f} \sim 10^{-5}$; the ratio of the duration of the loading (T) to the percolation $\left(\frac{H^2}{C_v} = \frac{\mu H^2}{KE(1+e)}\right)$, $\frac{TEK(1+e)}{\mu H^2} \sim 10^2$; the ratio of the duration of the loading (T) to the characteristic time of loading (period $\frac{1}{f}$), $Tf \sim 10^6$. It can be seen here that the loading duration is a very long time compared to the loading cycle and the characteristic time of percolation. The pore pressure in the sand layer has enough time to develop and to dissipation. Thus there is a small effect on the long time dynamic responses of the sand layer if the permeability coefficient changes in the limited range. The permeability coefficient is $K = \frac{\mu k}{\rho_w g} = 10^{-11}$, $k = 1 \times 10^{-4}$ cm/s, k is the Darcy permeability coefficient, the modulus of sand layer E is 5MPa, the characteristic length of the bucket H is 5 m, the gravity acceleration g is 10 m/s^2, the loading frequency f is 0.8Hz, the pore ratio of sand e is 0.67, the viscosity coefficient of water μ is 10^{-3} kg/(m s), the loading duration of ice-induced dynamic loading T is about 8.6×10^4s.

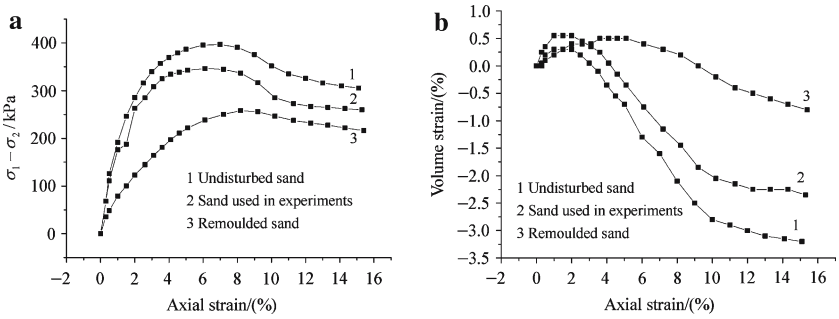

Fig. 1 Comparison of stress–strain relation of model sand, remoulded sand and undisturbed sand. **a** Axial strain versus stress difference ($\sigma_1 - \sigma_2$); **b** Axial strain versus volume strain

Table 2 Design of experiments

Experiment name	Amplitude	Size of bucket (Diameter × eight)/(cm × cm)	Block weight/g	Times of experiments
S1	Horizontal static load	6 × 7.2	98	1
S2	Horizontal static load	6 × 7.2	98	1
F1	10 N	6 × 7.2	98	
F2	40 N	6 × 7.2	98	3
F3	60 N	6 × 7.2	98	3
F4	20 N	6 × 7.2	98	1
L1	40 N	6 × 4.8	98	2
L2	60 N	6 × 9	98	1
W1	60 N	6 × 7.2	0	3
W2	40 N	6 × 7.2	166	1
V1	Vertical static load	6 × 4.8	0	2
VF1	2 mm	6 × 4.8	0	1
VF2	1 mm	6 × 4.8	0	1
VF3	0.5 mm	6 × 4.8	0	1
VF4	0.2 mm	6 × 4.8	0	1

3 Preparation of experiments

The experiments are performed in the 50 g-ton centrifuge in Tsinghua University. The maximum of the centrifugal acceleration is 200 g. The payload is 250 kg under 200 g.

The inner size of the model tank used in experiments is 60 m × 35 m × 35 cm. The experimental material is fine sand with special gravity 2.69, average grain diameter (D50) 0.014 cm and permeability coefficient 1×10^{-4} cm/s.

Some triaxial experiments are carried out to investigate the difference of mechanical properties between the model sand and the undisturbed sand. For comparison, the properties of remoulded sand are measured at the same time. The stress–strain curves and the volume curves are shown in Fig. 1. The properties of the model sand and the undisturbed sand are close.

Firstly, experiments under static loading are carried out to obtain the static bearing capacity which is a reference to the dynamic loading amplitude; Secondly, experiments under dynamic loading are carried out to investigate the dynamic responses of bucket foundations. The design for experiments is shown in Table 2. Some of the experimental results in Table 2 are chosen to discuss the responses under horizontal and vertical dynamic loading.

4 Experiments of static bearing capacity

A set of electro-hydraulic server loading system was used in the experiments for determining the horizontal static bearing capacity. The model bucket used in the static experiments had an inner diameter of 6 cm and a height of 7.2 cm. The layout of experiment is shown in Fig. 2. The horizontal displacement was measured by an LVDT located at 10 cm above the top of bucket on the fine pipe. A block with a weight of 0.098 kg was located at the top of the fine pipe to model the structural weight.

The horizontal loading was applied step by step. The loading increment in each step was 10 N. Loading was increased only when the development of displacement was almost steady in last step. The experiment was finished if the measured loading by force transducer decreased or kept a constant while the displacement increased.

Fig. 2 Layout for static bearing capacity experiment

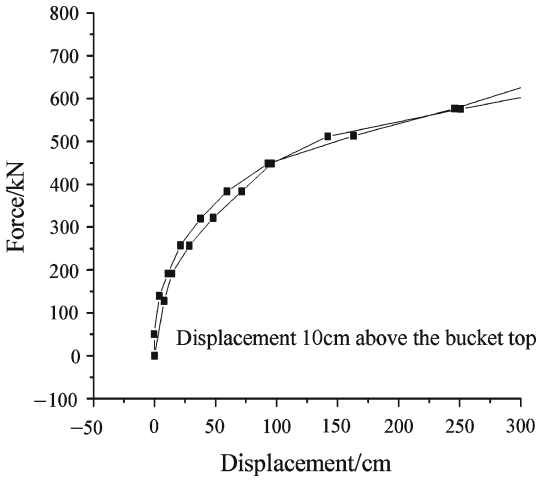

Fig. 3 Loading displacement curves

In Fig. 3, shown is the loading displacement curves of two repeated results for the experiments named S1 and S2. Their reliability is well. Each loading displacement curve may be divided into two parts: elastic deformation part or linear deformation part, and plastic deformation part or nonlinear deformation part. In the elastic deformation part, the loading displacement curve is almost linear, the deformation of bucket is small. The maximum of the loading in this part is about 2×10^5–3×10^5 N. In the plastic deformation part, the slope of the curve becomes smaller and smaller. The maximum of loading in this part is about 6×10^5–7×10^5 N.

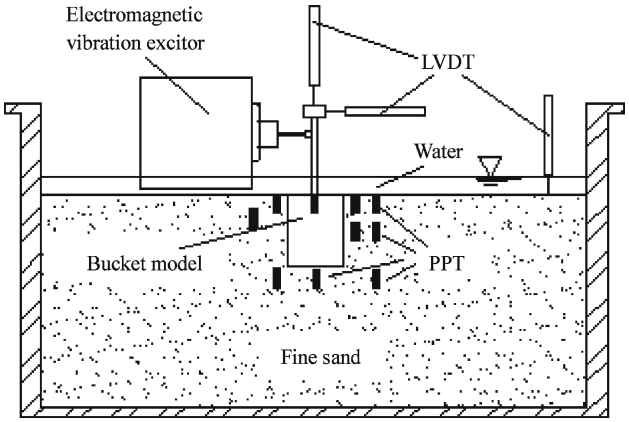

Fig. 4 Layout of the model

After finishing the static experiments, dynamic experiments were carried out. The layout of dynamic experiments is shown in Fig. 4. The sizes of three steel model buckets used in the experiments were of 4.8, 7.2 and 9.0 cm inner height with the 6.0 cm inner diameter. The thickness of both the wall and the top cap was 0.2 cm. A fine pipe with 0.8 cm inner diameter, 1.0 cm outer diameter and 11 cm length was welded at the center of the top cap. A sliding groove was closely connected with the pipe, which allowed a ball moving up and down to adapt the settlement of the bucket. One end of a steel pole was jointed with the ball. The other end of the pole was connected with the electromagnetic vibration exciter [26]. Thus the pole could not be dragged when the bucket settled. Two LVDT's were located at the top of the fine pipe to measure the vertical and horizontal displacements (Fig. 2). The other LVDT's were located on the sand layer surface to measure the settlements at different places. Ten PPT's, made in Druck Co. (English), were buried in the sand layer around and inside the bucket. The layout of PPT is shown in Fig. 5. The PPT's were not fixed but suspended in the sand layer.

In order to obtain the desired uniform density of the sand layer, the sand specimen is divided into several layers. The thickness of each layer is decided by the positions of PPT's. Each layer is compacted gently by hand to the given altitude decided the required dry density.

Fig. 5 Layout of the pore pressure transducers

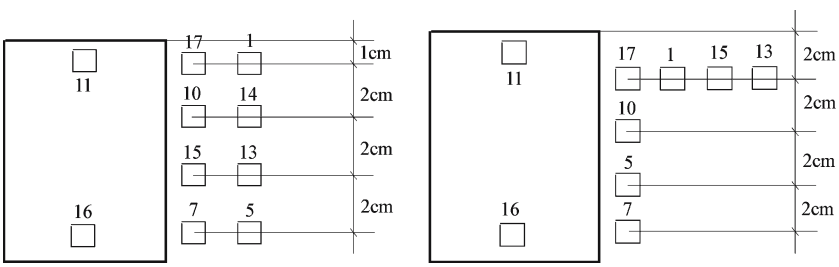

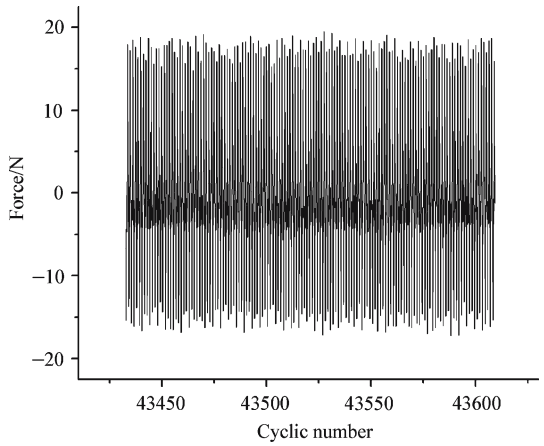

Fig. 6 Loading characteristics

After the dry sand sample was prepared, the sand layer was saturated by water from the bottom of the tank through a valve. A 2 cm thick coarse sand layer was laid at the bottom of the tank to allow the water to rise uniformly and prevent the piping till the water level was 1 cm over the sand layer surface. Vacuum was kept in the sand for 38 hour to increase the saturation degree after filling water. The saturated degree which was measured by the pore pressure was about 98% in the centrifugal tests. The saturated degree is the ratio of the pore pressure to that in full saturation condition.

After the saturation was completed, the consolidation was performed under consolidation pressure of 80 g. The dry densities before and after consolidation were 1.52 g/cm^3 and 1.6 g/cm^3, respectively, which were measured before and after consolidation when the centrifuge stopped according to the standards for geotechnical tests in SD 128-84 made by the Chinese Hydraulic and Electric' Department. The buoyant unit density was $\gamma' = 0.0971\,\text{kg/cm}^3$ after consolidation was finished. The consolidation curves of sand layer are presented in Fig. 7a. During consolidation, the pore pressure was measured to show the development of consolidation. When the settlement and the pore pressure did not increase anymore, consolidation was finished. It was found in experiments that the consolidation time that the sand density developed to 1.6 g/cm^3 and the settlement and pore pressure became stable was about 40 months.

The measured frequency of the platform caused by the dynamic ice-induced loading was 0.8–1.2 Hz in Bohai Bay, China. Accordingly, the frequency adopted in experiments was 0.8 Hz (in prototype). The loading point was 8 cm above the top of the bucket at the beginning. This relative position changed a little with the development of settlement. Steel blocks with different weights were located at the top of the fine steel pipe to model the structural weight. A typical loading characteristic is shown in Fig. 6.

5 Dynamic experimental results

5.1 The reliability of the experimental data

For the reliability of the experimental data, some experiments are repeated three or more times. In Fig. 7 shown are the reliability of the experimental results for the experiment named F4. In Fig. 7a shown are the results of settlements during consolidation. In Fig. 7b shown are the results of liquefaction index (the excess pore pressure is divided by the initial vertical effective stress) along depth for the 6.0 cm inner diameter and 7.2 cm height bucket with the loading amplitude of 60N and the frequency of 64 Hz. (If there is not indication, the data are in the model in the next subsections.)

5.2 The dynamic responses under horizontal loading

Under the dynamic loading, the pore pressure increases fast to the peak value at the first stage and then decreases to a steady state gradually. The dynamic responses (e.g. the excess pore pressure, the settlement) under different loading amplitudes are chosen for discussion (Figs. 8–11).

In Fig. 8 shown is the relation between the loading amplitude and the maximum of liquefaction index for the experiments named F1–F4. The maximum of the liquefaction index

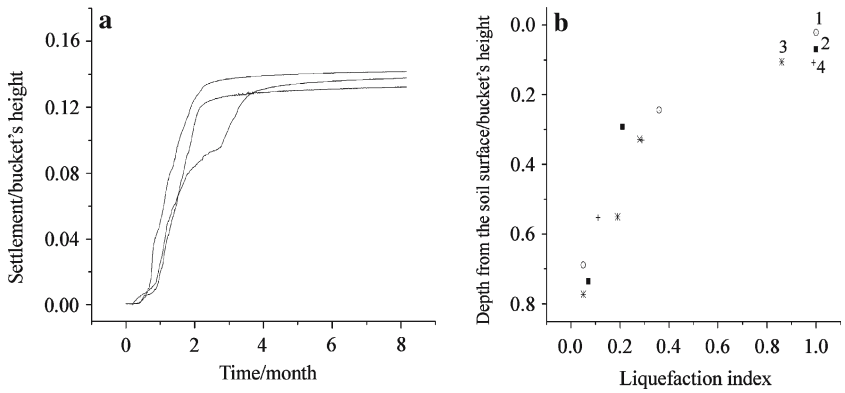

Fig. 7 The reliability of the experimental data. **a** Settlement (prototype); **b** Pore pressure along the depth

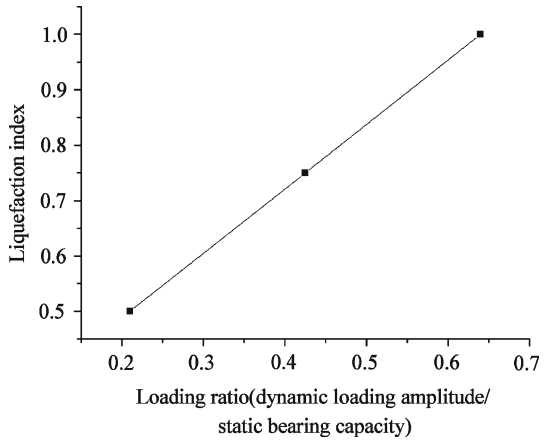

Fig. 8 The excess pore pressure versus loading amplitude

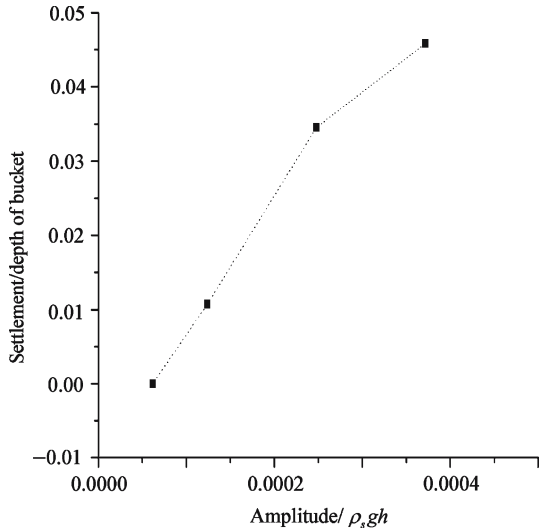

Fig. 9 The bucket's settlement versus loading amplitude

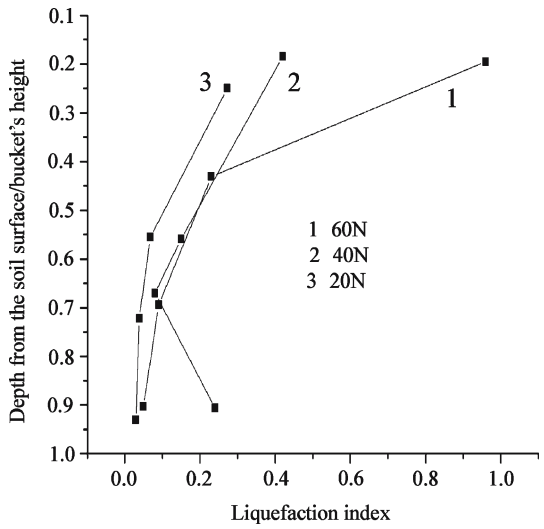

Fig. 10 The distribution of excess pore pressure along depth under different amplitudes

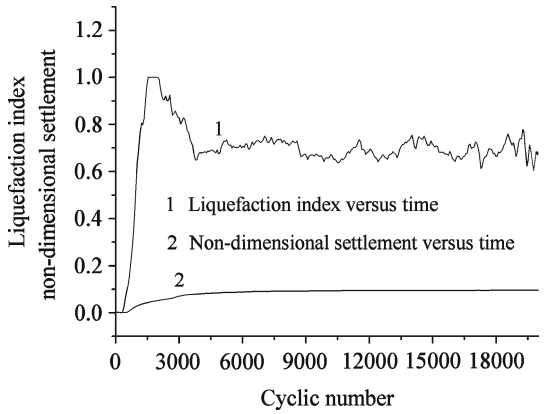

Fig. 11 Development of excess pore and settlement

increases with the increase of loading amplitude. The liquefaction index becomes smaller and smaller when the loading amplitude changes from 60 N (about 54% of the static bearing capacity) to 20 N (about 20% of the static bearing capacity). When the amplitude is 10 N (about 10% of the static bearing capacity), there is no building of the liquefaction index.

In Fig. 9 shown are the developments of bucket's settlement under different loading amplitudes for the experiments named F1–F4. When the loading amplitude is over a critical value, the settlement occurs. The settlements become smaller and smaller when the loading amplitude changes from 60 N (about 54% of the static bearing capacity) to 20 N (about 20% of the static bearing capacity). When the amplitude is 10 N (about 10% of the static bearing capacity), there is no settlement occurring.

In Fig. 10 shown is the distribution of excess pore pressure along depth under different loading amplitudes for the experiments named F1–F4. With the increase of the loading amplitude, the excess pore pressure in each point in the sand layer increases. The excess pore pressure decreases in the vertical direction from the sand layer surface. The sand layer is liquefied at shallow depth while the liquefaction index is only 0.08 at the level of the bucket's bottom. Within the thickness of 40% of the bucket's height in the sand layer, the excess pore pressure increases acutely. This may be why the bearing capacity does not lost completely when the loading lasts for a long time.

In Fig. 11 shown is the comparison of developments of the excess pore pressure and the bucket's settlement (here the data for the experiment named F3 is chosen for discussion). The liquefaction state will keep for a while after the sand layer is liquefied, then the excess pore pressure decreases to a steady state. During the development of sand layer from initial state to liquefaction, the settlement of bucket develops 30% of the total. When the pore pressure comes to a steady state, the settlement arrives at the maximum.

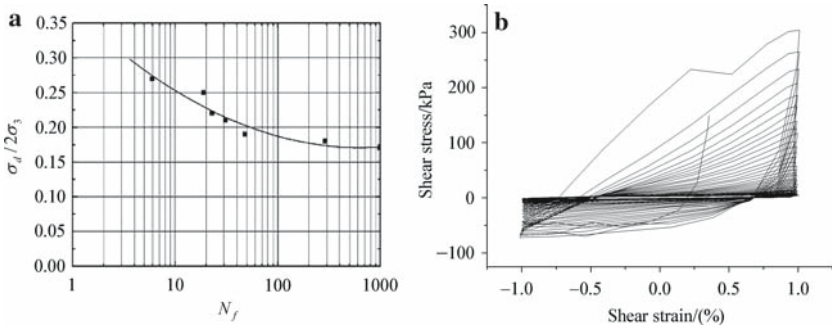

Fig. 12 The curve of liquefaction strength. **a** Stress ratio versus cyclic number; **b** Curve of stress and strain (In which $\sigma_d/2\sigma_3$ is the ratio of dynamic stress amplitude and confined pressure, $\sigma_d/2$ is the dynamic stress amplitude, σ_3 is the confined pressure, N_f is the cyclic number when the sand sample develops to liquefaction.)

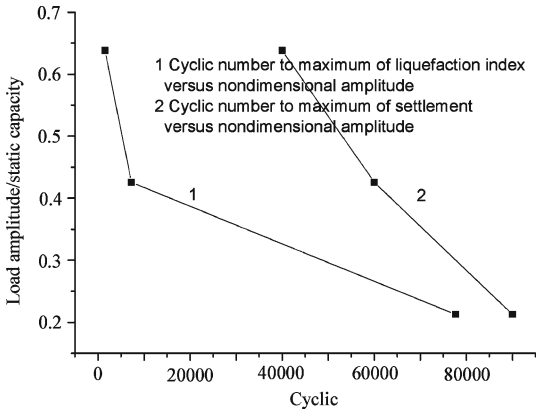

Fig. 13 Comparison of the time developing to the maximum of pore pressure and settlement

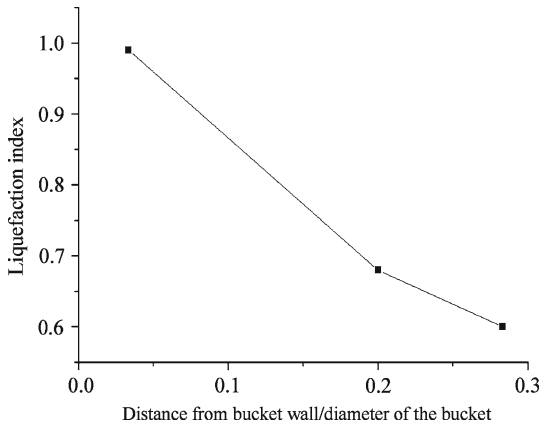

Fig. 14 The distribution of biggest excess pore pressure in horizontal direction

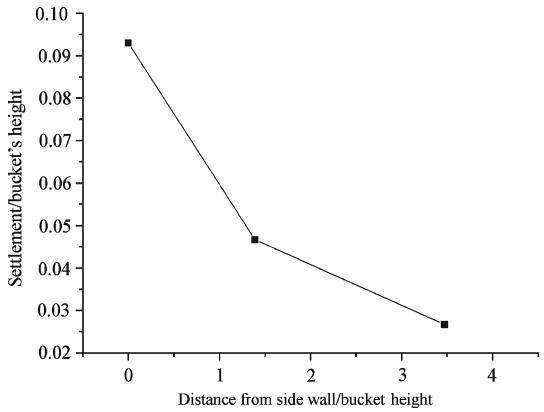

Fig. 15 Settlements of the bucket in horizontal direction

In Fig. 12 shown are the curve of liquefaction strength (the critical value may cause sand liquefied) and the relation of the strain and the stress of the model sand. These experiments for sand properties were carried out on a triaxial apparatus made in MTS (USA). The stress ratio (The amplitude of applied dynamic loading is divided by the initial vertical effective stress) increases with the decrease of cycle number needed for sand to liquefy. When the loading ratio is less than 15%, there is no liquefaction occurring. The strain will becomes bigger and bigger with the increase of cycle number. It indicates that there exist no liquefaction and settlement when the loading amplitude applied on the bucket is less than a critical value according to this figure. This value is decided by the critical stress ratio which may be obtained by the curve of liquefaction strength.

In Fig. 13 shown is the time developing to the maximum of pore pressure and bucket's settlement under different loading amplitudes for the experiments named F2–F4. It is shown that the time decreases while the time difference developing to the maximum pore pressure increases and the settlement increases with the increase of loading amplitude.

Figures 14 and 15 show the distribution of the maximum of pore pressure and settlement of sand layer in the horizontal direction. (Here the results of the experiment named F3 is chosen for discussion.) It is shown that the liquefaction index decreases roughly exponentially in the horizontal direction. The experiments show that the sand layer is liquefied under 1,200 cycles of 60 N cyclic loading at 1.44 cm depth (0.2 bucket height) and 0.2 cm away from the bucket's side wall, while the liquefaction index is only 0.4 at 1.7 cm away from the bucket's side wall. The settlements of the bucket and the sand layer at 8 and 20 cm away from the bucket's side wall are shown in Fig. 14. It is shown that the settlement decreases radially as function of the distance from the bucket's side wall.

As we all know, the disturbance born by the sand layer will become heavier with the increase of loading amplitude. Therefore, the excess pore pressure increases fast and high. At the first stage, the pore water is difficult to drain, so the pore pressure increases. The strength of the sand layer decreases and the sand layer is even liquefied with the increase of excess pore pressure. Nevertheless, the diffusion of the excess pore pressure will be over the generation gradually with the increase of the gradient of pore pressure. Accordingly, the sand layer settles and the pore pressure decreases.

During the sand layer's developing to liquefaction, the increase of pore pressure is larger than the dissipation. Therefore, the pore pressure may increase gradually while small settlement occurs. Once the sand layer is liquefied completely, the sand grains become suspending. After that, grains are solidified gradually from the lower part to the upper part. The excess pore pressure keeps constant during this stage. When the sand layer begins to consolidate, the pore pressure decreases gradually.

With the increase of loading amplitude, the liquefied layer thickness and the excess pore pressure in each point increase. Therefore, more time is needed to solidify and consolidate, which leads to the increase of time difference developing to the maximum between pore pressure and settlement.

5.3 Dynamic responses under vertical loading

The device for applying vertical loading is shown in Fig. 16. This device is a hydraulic-electric system and may output the vibration force amplitude 0–100 kg, or the vibration displacement amplitude 0–5 mm at the frequency of 20 Hz, and the frequency 0–20 Hz. The layout of the pore pressure transducers (PPT) is shown in Fig. 17. The uplift static bearing capacity is studied to obtain the stiffness and the criterion for choosing dynamic force amplitude before processing dynamic experiments. The load is applied by the way of displacement control. Each step increases by 0.2 mm. The curve of uplift static loading–displacement is given in Fig. 18 (Experiment V1). It is shown that the load increases fast with the increase of displacement. The uplift bearing capacity arrives at the displacement of 0.35 cm. After the peak, the load decreases a little. The bucket with a diameter of 6 cm and a height of 4.8 m is used in this experiment. The uplift bearing capacity is 60.1 kg.

Fig. 16 Picture of the vertical loading device

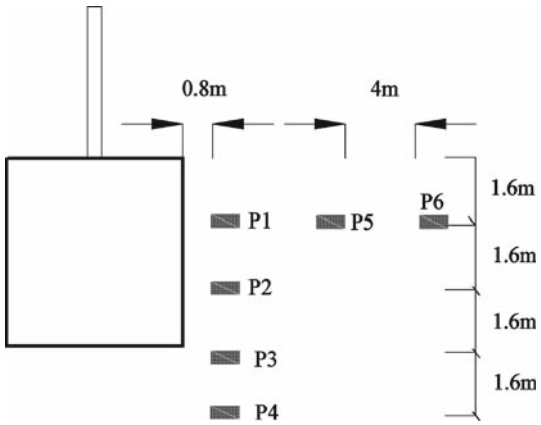

Fig. 17 Layout of PPT

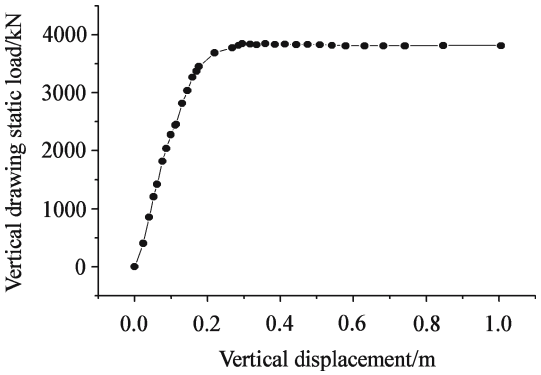

Fig. 18 Uplift load versus displacement

Figures 19–23 show the effects of the amplitude of vertical load on the dynamic responses for the experiments named VF1–VF4.

Figure 19 is the excess pore pressure development with time. It is shown that the pore pressure increases fast to a peak in 2–3 h, and then decreases gradually, which is similar to that under the horizontal dynamic loading.

Figure 20 is the distribution of excess pore pressure along the depth under the different load amplitudes. It is shown that the excess pore pressure decreases gradually along depth from the sand surface. The thickness of the liquefied sand layer in the upper part is enlarged with the increase of load

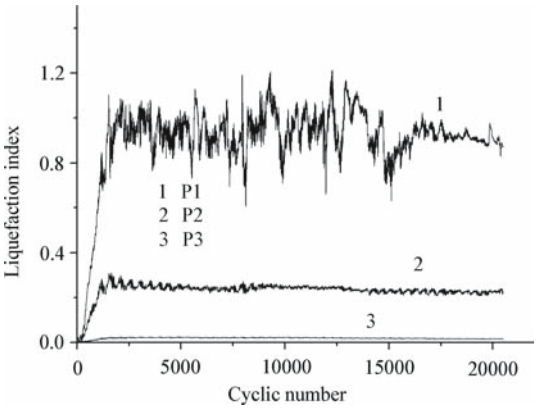

Fig. 19 Development of excess pore pressure with time (VF2: A = 1 mm)

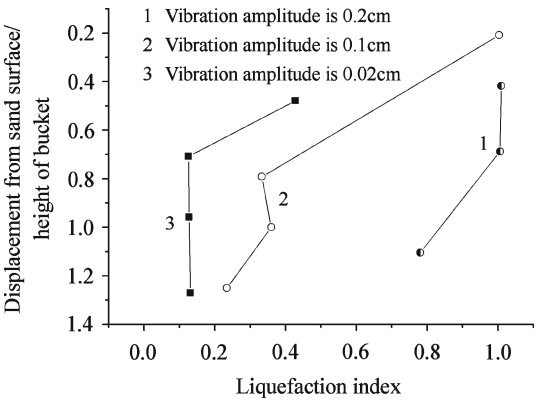

Fig. 20 Changes of excess pore pressure in the vertical direction

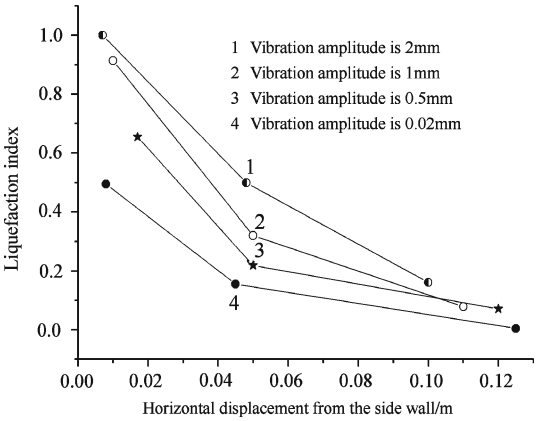

Fig. 21 Changes of excess pore pressure in the horizontal direction

amplitude. The sand from the surface to the bottom of the bucket is liquefied completely when the load amplitude is 2 mm (67% of the static bearing capacity).

Figure 21 is the distribution of excess pore pressure in the horizontal direction. It is shown that the excess pore pressure decreases from the bucket side wall to far away. The excess pore pressure increases in each place with the load amplitude.

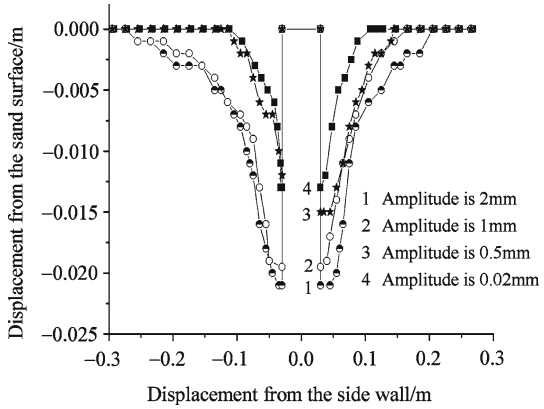

Fig. 22 Sand surface after experiment under different loading conditions

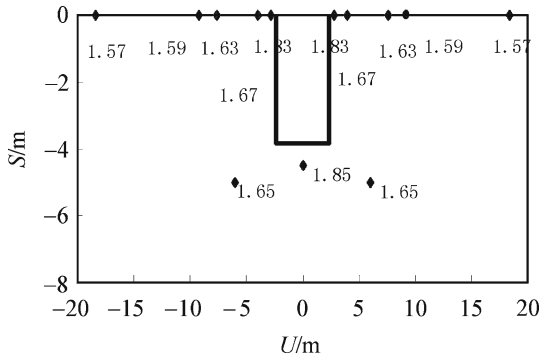

Fig. 23 The distribution of dry density after experiments in the center section (*U* denotes the distance from the center of bucket, *S* denotes the depth from surface.)

Figure 22 is the final place of the sand surface. It is shown that the maximum of the sand displacement increases with the load amplitude. Nevertheless, the maximum of the effected zone does not change with the load amplitude when it is over a critical value. It means that there is a limited effected zone around the bucket for a given sand layer. Inside the effected zone, the sand layer settles obviously, while outside the zone, the sand layer may be taken as elastic. It is shown that the sand density changes obviously in the limited zone, while the density changes little outside the zone by the distribution of density from Fig. 23. The reason is mainly that the liquefied sand has the filtering effect and damping effect, which lead effected zone being limited.

6 Conclusions

The centrifugal experiments were carried out to investigate the responses of bucket foundation under horizontal and vertical dynamic loading. It is shown that when the amplitude over a critical value (about 10%–18% of the static bearing capacity), the sand layer at the upper part (40% of the bucket's

height) around the bucket is softened or even liquefied under the horizontal dynamic loading while 100% of the bucket's height may be liquefied under the vertical dynamic loading. Because the upper part of sand layer near the bucket bears more disturbs, the excess pore pressure develops faster.

The excess pore pressure decreases along depth in the sand layer and decreases with distance from the bucket's side wall in the horizontal direction.

The excess pore pressure of the bucket with small height (with the same diameter) rises faster than the bucket with big height at each position.

The dynamic loading induces large settlement of the bucket. The settlement in the horizontal direction decreases steadily with the distance from the bucket's side wall.

There is a limited affected zone around the bucket inside which the settlement is obvious, while outside the zone, there is only elastic deformation.

Under a given condition, the dynamic responses develop to a steady state gradually. At this state, the pore pressure oscillation is at a steady average value, and the deformation does not develop.

References

1. Clukey, E.C., Morrison, M.J., Garnier, J., et al.: The response of suction caissons in normally consolidated clays to cyclic TLP loading conditions. In: Proceedings of Offshore Technology Conference, Houston, OTC 7796, pp. 909–918 (1995)
2. Allersma, H.G.B., Plenevaux, F.J.A.: Wintgens JFPCME: simulation of suction pile installation in sand in a geocentrifuge. In: Proceedings of the 7th International Offshore and Polar Engineering Conference (ISOPE97), 1:761–765 (1997)
3. Allersma, H.G.B., Kierstein, A.A., Maes, D.: Centrifuge modeling on suction piles under cyclic and long term vertical loading. In: Proceedings of 10th International Offshore and Polar Engineering Conference, Seattle, USA, International Society of Offshore and Polar Engineers (2000)
4. Housby, G.T., Byrne, B.W.: Suction caisson foundations for offshore wind turbines and anemometer masts. Wind Eng. **24**(4), 249–255 (2000)
5. Byrne, B.W., Housby, G.T., Martin, C.M., Fish, P.M.: Suction caisson foundations for offshore wind turbines. Wind Eng. **26**(3), 145–155 (2002)
6. Byrne, B.W., Houlsby, G.T.: Experimental investigations of the responses of suction caissons to transient combined loading. ASCE J. Geotech. Geoenviron. Eng. **130**(3), 240–253 (2004)
7. Andersen, K.H., Jostad, H.P.: Foundation design of skirted foundations and anchors in clay. In: Proceedings of Offshore Technology Conference, Houston, Texas, OTC 10824, pp. 1–10 (1999)
8. Housby, G.T., Puzrin, A.M.: A thermomechanical frame-work for constitutive models for rate-independent dissipative materials. Int. J. Plast **16**(9), 1017–1047 (2000)
9. Senpere, D., Auvergne, G.A.: Suction anchor piles-a proven alternative to driving or drilling. In: Proceedings of Offshore Technology Conference, Houston, OTC4206, pp. 483–493(1982)
10. Aas, P.M., Andersen, K.H.: Skirted foundation for offshore structure. In: Proceedings of the 9th Offshore South East Asia Conference, Singapore. World Trade Center Singapore, Singapore, pp. 1–7, (1992)
11. Dyme, W., Houlsby, G.T.: Drained behavior of suction caisson on very dense sand. In: Proceedings of Offshore Technology Conference, Houston, OTC10994, pp. 765–782 (1998)
12. Tjelta, T.L., Hermstad, J., Andenaes, E.: The skirt piled gullfaks c platform installation. In: Proceedings of Offshore Technology Conference, Houston, OTC6473, pp. 453–462 (1990)
13. Bye, A., Erbrich, C., Earl, K., et al.: Geotechnical design of bucket foundation. In: Proceedings of Offshore Technology Conference, Houston, OTC7793, pp. 869–883(1995)
14. Tjelta, T.I., Guttormsen, T.R., Hermstad, J.: Large-scale penetration test at a deepwater site. In: Proceedings of Offshore Technology Conference, Houston, OTC 5103, pp. 201–212 (1986)
15. Clukey, E.C.: Suction caisson design issues. OTRC 2001, In: Proceedings of the International Conference Geotechnique, Geological and Geophysical Properties of Deepwater Sediments, Houston, pp. 163–181 (2001)
16. Cassidy, M.J., Byrne, B.W., Randolph, M.F.: A comparison of the combined load behavior of spudcan and caisson foundations on soft normally consolidated clay. Geotechnique **54**(2), 91–106 (2004)
17. Fugsang, L.D., Steensen-Bach, J.O.: Breakout resistance of suction piles in clay. In: Ko, H.Y., Mclean, F.G. (eds.) Proceedings of the International Conference: Centrifuge 91. A.A. Balkema, Rotterdam, The Netherlands, 153–159 (1991)
18. Jones, W.C., Iskander, M.G., Olson, R.E., et al.: Axial capacity of suction piles in sand. In: Chryssostomidis, C. (ed.) Proceedings of 7th International Conference on the Behavior of Offshore Strucutres. Pergamom, pp. 63–75 (1994)
19. Steensen-Bach, J.O.: Recent model tests with suction piles in clay and in sand. In: Proceedings of Offshore Technology Conference, Houston, OTC6844, pp. 323–330 (1992)
20. Luke, A.M., Rauch, A.F., Olson, R.E., et al.: Components of suction caisson capacity measured in axial pullout tests. Ocean Eng. **32**, 878–891 (2005)
21. Ding, H.Y., Qi, L., Du, X.Z.: Estimating soil liquefaction in ice-induced vibration of bucket foundation. J. Cold Reg. Eng. **17**(2), 60–67 (2003)
22. Lu, X.B., Zheng, Z.M., Zhang, J.L.: Progress in the study on the bucket foundation of offshore platform. Adv. Mech. **33**(1), 27–40 (2003) (in Chinese)
23. Housby, G.T., Byrne, B.W.: Design procedures for installation of suction caissons in sand. Geotech. Eng. **158**(GE3), 135–144 (2005)
24. Housby, G.T., Byrne, B.W.: Design procedures for installation of suction caissons in clay and other materials. Geotech. Eng. **158**(GE2), 75–82 (2005)
25. Taylor, R.N.: Geotechnical Centrifuge Technology. Blackie Academic & Professional, London (1995)
26. Lu, X.B., Zhang, X.H., Sun, G.L., et al.: Simulation of dynamic loading in centrifuge modeling for suction bucket foundations. In: Proceedings of 15th International Offshore and Polar Engineering Conference (ISOPE), 19–24 June 2005, 2:423–430